Sensor Applications

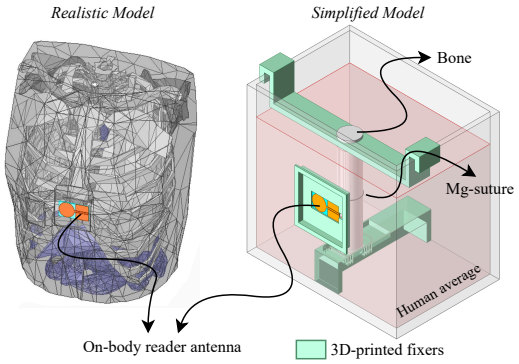
Wireless Monitoring of Mg-6Ag Alloy based Biodegradable Sternal Sutures with an On-body Antenna

Ozge Taylan Moral[1*], Ahmet Bilir[2*], Benay Uzer[3], Bjorn Wiese[4] and Sema Dumanli[1**]

[1] *Department of Electrical and Electronics Engineering, Bogazici University, Istanbul, 34342, Turkey*
[2] *Department of Electrical Engineering, École Polytechnique Fédérale de Lausanne, Lausanne, Switzerland*
[3] *Department of Mechanical Engineering, Izmir Institute of Technology, Izmir, 35430, Turkey*
[4] *Materials Technology and Innovation, Helmholtz-Zentrum hereon GmbH, Geesthacht, Germany*
[*] *Student Member, IEEE*
[**] *Senior Member, IEEE*

Manuscript received June 7, 2017; revised June 21, 2017; accepted July 6, 2017. Date of publication July 12, 2017; date of current version July 12, 2017.

Abstract—This paper presents a wireless sensing system to monitor the structural integrity of magnesium-silver alloy based biodegradable sutures, specifically designed for sternal applications. A body-matched ultra-wideband coplanar waveguide-fed circular disc monopole antenna is designed to propagate into the complex lossy medium of the human torso. It detects structural changes in a loop-shaped suture by monitoring variations in return loss characteristics, enabled by coupling between the antenna and the suture. The system performance is validated via simulations and measurements with numerical and physical phantoms, including analyses for suture-antenna misalignment and suture depth. Moreover, the on-body antenna successfully monitors accelerated suture degradation in an acidic tissue-mimicking phantom, simulating long-term effects. It has been shown that degradation can be detected up to a depth of 20 mm in the body. This approach enables non-invasive, real-time feedback on sternal healing, potentially improving post-operative care and patient outcomes.



Index Terms—Biodegradable implants, biodegradable sutures, on-body antenna, wearable antenna, wireless sensing.

I. INTRODUCTION

Surgical sutures are key medical devices for wound closure, tissue repair, and prosthesis fixation, with selection based on the specific surgical procedure [1], [2]. For sternal closure, metallic wires—typically stainless steel—are the clinical standard due to their durability, but removal of the suture after treatment could damage the healed tissue. Furthermore, corrosion initiated by infection or body fluids can trigger adverse reactions due to the release of metal ions [3]. Here, we focus on biodegradable sutures, which have emerged as a promising alternative to overcome these limitations.

Mg and their alloys have recently been studied as biodegradable implant metals [4]. Mg alloys are especially promising due to their low density, high biocompatibility, good strength-to-weight ratio, damping capacity, and bone-like elastic modulus, which helps reduce stress shielding [5]. However, they have lower mechanical strength than traditional metal implants and may degrade rapidly, releasing hydrogen, which strongly depend on the alloy composition and processing. Various alloying systems such as RE, Ca, Zn, Al, and Ag—have been explored to improve degradable Mg-based materials. In the case of Ag, it offers an additional antimicrobial effect [6], [7] that makes it suitable for implants with a large surface area, such as open porous scaffolds or wire-based sutures. Regarding material properties, Ag in Mg also improves deformation properties [8], which are advantageous both in the manufacture of wires and when used as a suture material due to the higher ductility resulting. In vitro tests of Mg-Ag materials showed no negative effects on cells [6], [7], [9] making them promising candidates for medical use. In [10], it was shown that small precipitations can be critical for the service life of Mg wires. Another study also presented that impurities from the manufacturing and handling of Mg can lead to contamination with Fe from the tools [11], [12]. This, therefore, has a dramatic effect on the degradation or corrosion behavior of Mg. To safely establish new medical technologies as the standard, precise control of the degradation process is essential. Therefore, real-time monitoring in animals and later in humans would be very helpful.

Ensuring the structural integrity of Mg implants during healing can be achieved by real-time monitoring using spectroscopic [13], optical [14], and chemical sensors [15], as well as biosensors [16]. Since these systems are based on detecting corrosion byproducts and often require complicated setups, they are unsuitable for portable, continuous real-time monitoring.

The interaction between the medical implants and on-body wireless devices can be utilized for wireless monitoring of implants since electromagnetic waves interact with the medium they propagate in. For example, [17] studies the effects of the steel sternotomy wires on the on-body channel response, corresponding antenna location and wire embedding through simulations. Similarly, [18] investigates the impact of sternotomy wires and aortic valve implants on the radio channel characteristics, for on-body and off-body communications. Although wireless monitoring was not an aim in these studies, the

Corresponding author: S. Dumanli. (e-mail: sema.dumanli@bogazici.edu.tr)
Associate Editor: Alan Smithee.
Digital Object Identifier 10.1109/LSENS.2023.0000000

Table 1: The proposed study with related studies

Ref.	Application	Sensing Element	Biodegradable	Readout	Freq. / Depth
[19]	Soft-tissue monitoring	PLA-based implant	Yes	Dual horn antenna	4.8–8.1 GHz / 10 mm (simulation in fat layer)
[20]	Arterial pulse monitoring	Mg + polymer sensor	Yes	Reader coil	app. 650 - 800 MHz / Subcutaneous (in vivo)
[21]	Infection monitoring	Mg implant antenna	Yes	Wearable slot antenna	1.5 GHz / 10 mm (ex vivo)
[22]	Suture strain monitoring	Ag/polyurethane fiber strain sensor	No	Wired electrical	N/A / Porcine skin (ex vivo)
[23]	Deep-wound integrity	PEDOT:PSS-functionalized silk suture	No	Dipole antenna	1-2 GHz Tx/ 2-4 GHz Rx / ~20 mm (in vivo) / 40 mm (ex vivo)
[24]	Suture-anchor tension monitoring	Semiconductor strain gauge + LCR sensor	No	Inductive detection coil	14.4 - 19.8 MHz / 20 mm (ex vivo)
[25]	Suture loading	PLA suture pledget + LC sensor	Not fully	Inductive detection coil	app. 410 MHz / 16 mm (tissue-mimicking phantom)
This work	**Suture degradation**	**Mg-6Ag suture**	**Yes**	**CPW-circular monopole antenna**	**808–830 MHz / 20 mm (tissue-mimicking phantom)**

results show that the presence of the implant affects the channel impulse response. Therefore, it can be concluded that the degradation of a Mg implant can be wirelessly monitored using an on-body antenna. In [19], a biodegradable implant is developed to monitor soft tissue healing based on chipless RF-ID technology. A biodegradable and flexible arterial-pulse sensor operating in a similar way is proposed in [20], providing real-time post-operative blood flow monitoring. And [21] proposes a Mg-based implant antenna for biodegradation tracking, and a wearable slot antenna is used to monitor the state of the implant antenna. These implantable systems include a resonating structure that is designed to operate at a specific frequency of operation. Although we have a similar approach, in this paper the suture loops fixed around the sternum is not shaped to resonate at a specific frequency, but their naturally occurring resonance is tracked. On the other hand, there are studies that propose the use of smart sutures to monitor postoperative care and wound management [22]–[25]. Unlike the suture in the proposed system, these functionalized sutures used within or on the body are not fully biodegradable due to the sensing mechanisms they incorporate.

This paper investigates the possibility of using an on-body reader antenna to wirelessly monitor the structural integrity of a Mg-6Ag alloy based suture and its degradation during the healing process. A single loop is used and its size is dictated by the sternum in the numerical phantom. The monitoring is differential, hence the size of the loop is not critical. The proposed system offers portable, real-time, continuous monitoring using non-ionizing electromagnetic waves in the microwave frequency range, which are considered safe for the human body for limited transmission power levels. A comparison of the proposed study with related studies is presented in Table 1.

II. BODY-MATCHED ANTENNA DESIGN

A circular disc monopole antenna is designed on Rogers RO3210 with a relative permittivity (ϵ_r) of 10.2 and fed by 50 Ω coplanar-waveguide (CPW). While the base topology is inspired by [26], the proposed antenna is specifically engineered to propagate into a lossy human torso that couples with the loop-shaped suture. The high dielectric constant of RO3210 was selected to facilitate antenna miniaturization, while the standard 1.27-mm substrate thickness provides a practical compromise between mechanical robustness and profile. The body-matched antenna is modeled and optimized on a realistic human model in ANSYS HFSS (2023 R2), and the antenna geometry with optimized final dimensions can be seen in Fig. 1a. Under such a complex dielectric load, the operating bandwidth of the body-matched antenna is highly sensitive to the feed gap, ground plane width, and disc radius. The trace width and ground spacing were tuned to 0.8 and 2.5 mm, respectively, to maintain the 50 Ω impedance matching. These variable are mainly chosen to optimize the antenna for on-body operation. The on-body reader antenna is fabricated on a single layer of 1.27-mm Rogers RO3210 using an LPKF S103 as seen in Fig. 1b. The reflection coefficient of the

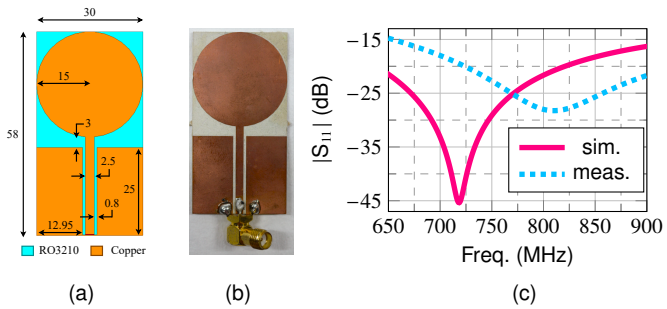


Figure 1: (a) The geometry of the antenna. Note that the units are in mm. (b) The prototyped antenna. (c) Simulation and measurement results of on-body antenna on the human average phantom.

prototyped antenna is measured using a Rohde & Schwarz ZNLE6, calibrated within 500 – 1000 MHz frequency range. The simulated and measured reflection coefficients of the on-body antenna for the operation on the human average phantom are depicted in Fig. 1c.

III. WIRELESS MONITORING

A. Simulation Model

The numerical study of the proposed system is conducted with both the realistic human phantom and a simplified phantom, as seen in Fig. 2a. The realistic human phantom model has been simplified while preserving parameters such as the electrical properties and the total dimensions of the human body, as well as the depth and size of the sternum, to decrease the computational cost and to extend the analysis for people of different weights simply by changing the depth of the bone. The simplified phantom includes a $20 \times 30 \times 24$ cm box and a cylinder with a radius of 20 mm and a height of 20 cm. The box (human torso) and the cylinder (sternum) are assigned the frequency-dependent dielectric properties of human average and bone, respectively, from the ANSYS HFSS material library. The on-body antenna performed similarly on both phantoms, with a first resonant frequency of 0.71 GHz on the realistic model and 0.72 GHz on the simplified model. Since the tracking is going to be conducted using the reflection coefficient, the simplified model is considered acceptable.

For the numerical study, the measurement setup is modeled in ANSYS HFSS, as seen in Fig. 2a. The model consists of the simplified phantom, the suture, a plexiglass container, fixers for bone depth adjustment, and a holder to fix the on-body antenna. Surrounding the sternum, the suture is modeled as a metal loop of 20 mm radius, 1 mm^2 square cross-section, that is located at the center of the bone and aligned with the antenna. Using this model, the following numerical analyses are performed: First, the wireless sensing of the biodegradation is demonstrated by comparing the return loss of the on-body antenna at the initial and final stages of the biodegradation for implant depths, defined as the distance from the antenna to the implant, of 15 and 20 mm to take the variation from patient to patient

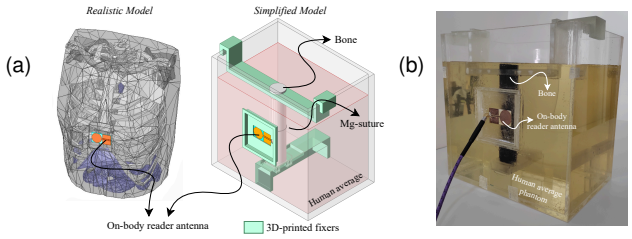


Figure 2: (a) The realistic and simplified simulation models. (b) The measurement setup.

into account. Secondly, predicted variations in a realistic scenario are analyzed where there is on-body antenna misalignment. The sternum is located at depths of 15 and 20 mm, and the suture is positioned in the middle of the bone, aligned with the antenna. The antenna response is then examined by moving the suture 25 mm above and below. The results of these analyzes are given in the section IV. To ensure tissue safety for the proposed system, the maximum simulated Specific Absorption Rate was evaluated at a 10 mW input power, yielding 0.649 W/kg and 0.242 W/kg for 1-g and 10-g averaging, respectively, which are well within the applicable safety limits.

B. Measurements on Tissue-mimicking Phantoms

As shown in Fig. 2b, the measurement setup consists of a plexiglass container with phantom materials, 3D-printed fixers, and an on-body antenna that is placed using a 3D-printed holder. The suture samples used in this study were manufactured from Mg-6Ag alloy. A detailed description of the production of Mg alloy with 6 wt.% Ag, the casting process, and the chemical composition is published in [8]. The ingot was machined to a diameter of 49 mm and a length of 150 mm. This ingot was homogenized at 450 °C for 16 hours and quenched in water. After preheating to the extrusion temperature of 425 °C for 1 hour, the ingot was pressed with a ram speed of 0.2 mm/s. The container used had a diameter of 50 mm, and the die had 4 holes, each with a diameter of 1 mm. The wire diameter achieved for this investigation was 0.98 mm.

The tissue-mimicking phantom for human average was prepared using deionized water of 4000 mL, granulated sugar of 8000 g, salt of 160 g and sodium azide of 13.33 g. Sugar decreases ϵ_r, salt increases σ, and sodium azide prevents mold growth. The phantom for human bone was fabricated from carbon black of 6.75 g, graphite of 40 g, and E-50 RTV-2 silicone of 450 g. Carbon black increases both ϵ_r and σ, while graphite increases primarily ϵ_r. The electrical properties of the fabricated phantoms were validated at 725 MHz with a dielectric assessment kit SPEAG DAK-3.5. A comparison of the electrical properties of the numerical and physical phantoms for human average and human bone is shown in Fig. 3. Within the band of interest, the maximum deviations of ϵ_r and σ for the human average phantom are 2.78% and 0.82%, respectively, while these values are 6.93% and 0.16% for the human bone phantom. For both phantoms, they mimic the targeted tissues well.

IV. RESULTS AND DISCUSSION

The degradation is sensed through the magnitude of the return loss of the on-body antenna. Fig. 4. presents the difference in return loss between the initial (suture present) and final (fully degraded suture) stages of biodegradation for 15 and 20 mm depths. The resonant frequency shifts are 35 and 17 MHz at distances of 15 and 20 mm, respectively. These simulations are validated through

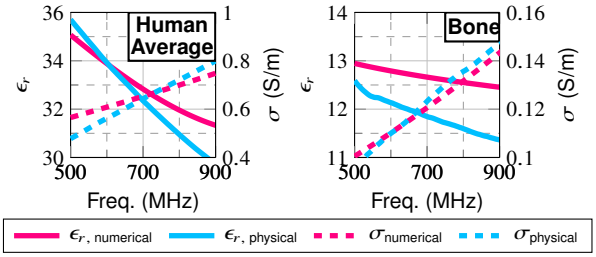


Figure 3: The frequency-dependent electrical properties of numerical [27] and physical human average and bone phantoms.

measurements, as plotted in Fig. 4. After degradation, the resonant frequency shifts are 25 and 1 MHz at distances of 15 and 20 mm, respectively. The degradation can be detected up to 20 mm with measurements as predicted by the simulations. It has been observed that the degradation of suture can be sensed for individuals with different body weights. Fig. 5. presents the change in reflection coefficient of the on-body antenna as the suture height is changed by 25 mm. This simulation result shows that misalignment severely affects the sensing capability. The shift caused by the misalignment is greater than the shift caused by the degradation. Accordingly, stable antenna positioning is essential for practical implementation, while patient-specific baseline calibration may help account for anatomical variability and placement-dependent detuning.

In order to monitor the degradation of the suture in real time in a shorter time period, the human average phantom is made acidic with citric acid monohydrate of 292.30 g. The pH value of the mixture was reduced from 6.58 to 2.30, which led to minimal changes in the dielectric properties of phantom. The degradation of the suture is then monitored in real time for 36 hours as the suture reacts with the acidic phantom. As seen in Fig. 6, the resonant frequency changed at 16, 23, and 33 hours when the suture lost integrity on the posterior, lateral, and anterior surfaces, respectively. Although the complete 36-hour degradation cycle was not independently repeated, the observed baseline variation was approximately ±2 MHz, mainly attributed to environmental and instrumental fluctuations, and remained substantially smaller than the overall 23 MHz degradation-induced resonance shift. Phantom-based and accelerated degradation conditions do not fully replicate physiological degradation rates or in vivo complexity; validation under representative conditions remains future work.

V. CONCLUSION

This study demonstrates a non-invasive wireless sensing system designed to monitor the structural integrity of biodegradable Mg-6Ag based sutures. A body-matched UWB CPW-fed circular disc monopole antenna is designed to propagate into human body. It is aligned and coupled to the loop shaped suture. Through numerical analysis and measurements, the effect of the degradation or breakage of the suture on the body-matched antenna's input response is presented. And the impact of suture depth and misalignment is investigated. Furthermore, by employing acidic phantoms to create an accelerated degradation environment, the system successfully monitored the actual degradation state of the suture beyond mere presence, demonstrating high sensitivity to real-time structural changes in the suture. A monitoring depth of 20 mm has been achieved, and hence the system requires patients' pre-sternal tissue thickness to be under this limit for clinical applications. While this study validates

the sensing mechanism under controlled conditions, future in-vivo studies will address the impact of dynamic physiological factors on the system's reliability. Future work will investigate a flexible, conformal implementation to reduce air gaps with the curved body surface and mitigating placement-related misalignment, potentially enhancing electromagnetic coupling and sensing accuracy.

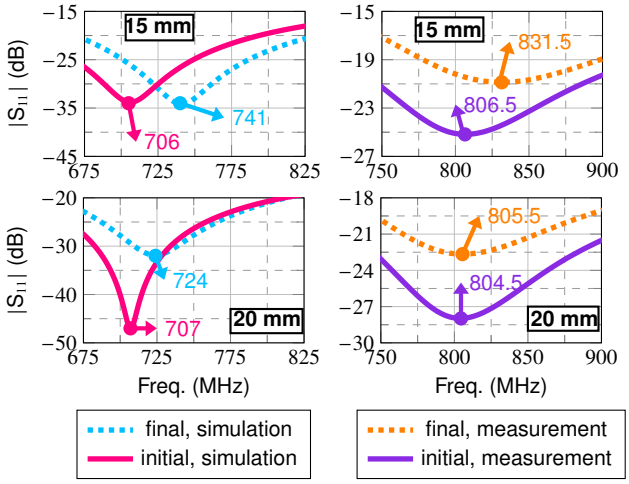


Figure 4: Degradation analysis: simulation and measurement results for different distances between the on-body antenna and the suture.

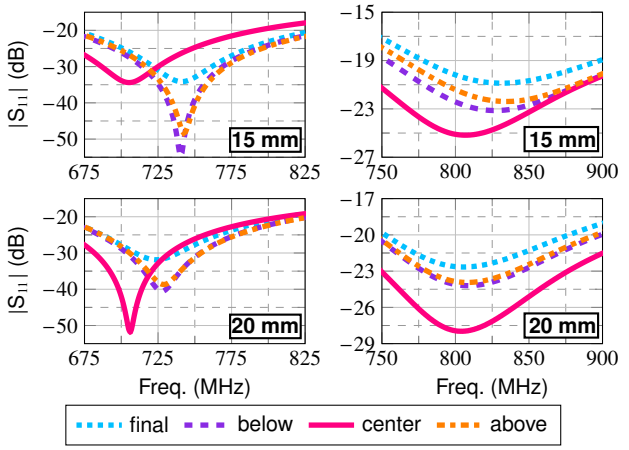


Figure 5: Misalignment analysis: simulation (left) and measurement (right) results for different alignment positions of the suture relative to the on-body antenna.

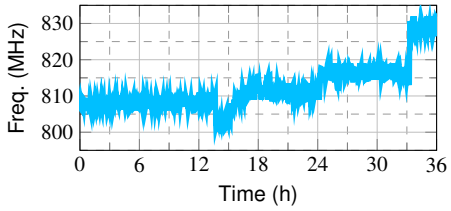


Figure 6: The resonant frequency of the on-body reader antenna in the acidic human average phantom over 36 hours.

ACKNOWLEDGMENT

The authors thank Ozan F. Sezgen, Anil Tulu, Burak F. Ozcan, and Mehmet E. Korkmaz for their help with phantom preparation, 3D printing, and measurements.

REFERENCES

[1] H. Aravind, "Suture materials, emerging trends," in *Advanced Technologies and Polymer Materials for Surgical Sutures,* UK: Woodhead, 2023, pp. 237–247.

[2] A. K. Narasimhan, T. S. Rahul, and S. Krishnan, "Revisiting the properties of suture materials: an overview," *Advanced Technologies and Polymer Materials for Surgical Sutures,*, UK: Woodhead, 2023, pp. 199–235.

[3] Y. Li et al., "Advances, challenges, and prospects for surgical suture materials," *Acta Biomater.*, vol. 168, pp. 78–112, 2023.

[4] J. M. Seitz, M. Durisin, J. Goldman, and J. W., Drelich, "Recent advances in biodegradable metals for medical sutures: A critical review," *Adv. Healthcare Mater.*, vol. 4, no. 13, pp. 1915–1936, 2015.

[5] B. Uzer-Yilmaz, "Mechanical performance of metallic biomaterials: Fundamentals and mechanisms," in *Multiscale Cell-Biomaterials Interplay in Musculoskeletal Tissue Engineering and Regenerative Medicine*, Academic Press, 2024, pp. 113–126.

[6] D. Tie et al., "Antibacterial biodegradable Mg-Ag alloys," *Eur. Cell. Mater.*, vol. 25, pp. 284 – 298, 2013.

[7] Z. Liu et al., "Influence of the microstructure and silver content on degradation, cytocompatibility, and antibacterial properties of magnesium-silver alloys in vitro," *Oxid. Med. Cell. Longev.*, art. no. 8091265, 2017.

[8] B. Wiese, R. Willumeit-Römer, D. Letzig, and J. Bohlen, "Alloying effect of silver in magnesium on the development of microstructure and mechanical properties by indirect extrusion," *J. Magnes. Alloys.*, vol. 9, no. 1, pp. 112 – 122, 2021.

[9] I. Marco et al., "In vivo and in vitro degradation comparison of pure MG, MG-10GD and MG-2AG: A short term study," *Eur. Cell. Mater.*, vol. 33, pp. 90 – 104, 2017.

[10] S. Meyer et al., "Degradation analysis of thin mg-xag wires using x-ray near-field holotomography," *Metals.*, 11 (9), art. no. 1422, 2021.

[11] M. M. Gawlik, B. Wiese, V. Desharnais, T. Ebel, and R. Willumeit-Römer, "The effect of surface treatments on the degradation of biomedical Mg alloys-a review paper," *Materials.*, 11 (12), art. no. 2561, 2018.

[12] M. M. Gawlik et al., "Acetic acid etching of Mg-xGd alloys," *Metals.*, 9 (2), art. no. 117, 2019.

[13] H. W. Hassan, M. Rahmati, A. Barrantes, H. J. Haugen and P. Mirtaheri, "In vitro monitoring of magnesium-based implants degradation by surface analysis and optical spectroscopy," *Int. J. Mol. Sci.*, vol. 23, no. 11, art. no. 6099, May. 2022.

[14] A. Mathew et al., "In vivo analysis of a biodegradable magnesium alloy implant in an animal model using near-infrared spectroscopy," *Sensors.*, vol. 23, no. 6, art. no. 3063, Mar. 2023.

[15] D. Zhao et al., "Visual hydrogen mapping sensor for noninvasive monitoring of bioresorbable magnesium implants in vivo," *JOM.*, vol. 72, pp. 1851–1858, May. 2020.

[16] M. Su Natasha, R. S. P. Malon, D. H. Wicaksono, E. P. Córcoles, and H. Hermawan, "Monitoring magnesium degradation using microdialysis and fabric-based biosensors." *Sci. China Mater.*, vol. 61, pp. 643–651, Aug. 2018.

[17] M. Särestöniemi, C. Pomalaza-ráez, Z. Bi, T. Kumpuniemi, C. Kissi, and M. Sonkki, "Comprehensive study on the impact of sternotomy wires on UWB WBAN channel characteristics on the human chestArea," *IEEE Access.*, vol. 7, pp. 74670–74682, May. 2019.

[18] M. Särestöniemi, C. Pomalaza-ráez, T. Kumpuniemi, M. Hämäläinen, R. Kovacs, and J. Iinatti, "Measurement data-based study on the intrabody propagation in the presence of the sternotomy wires and aortic valve implant," *IEEE Trans. Antennas Propag.*, vol. 67, no. 8, pp. 4989–5001, 2019.

[19] J. M. Rigelsford, B. F. Al-Azzawi, C. J. Davenport, and P. Novodvorsky, "A passive biodegradable implant for subcutaneous soft-tissue trauma monitoring," *IEEE J. Biomed. Health Inform.*, vol. 19, no. 3, pp. 901–909, 2015.

[20] C. M. Boutry et al., "Biodegradable and flexible arterial-pulse sensor for the wireless monitoring of blood flow, " *Nat. Biomed. Eng.*, vol. 3, no. 1, pp. 47–57, 2019.

[21] K. Ararat, O. Altan, S. Serbest, O. Baser, and S. Dumanli "A biodegradable implant antenna detecting post-surgical infection," in *Proc. 14th Eur. Conf. Antennas Propag. (EuCAP)*, Copenhagen, Denmark, 2020, 1–4.

[22] Y. Lee et al., "A multifunctional electronic suture for continuous strain monitoring and on-demand drug release," *Nanoscale.*, vol. 13, no. 43, pp. 18112–18124, 2021.

[23] V. Kalidasan et al., "Wirelessly operated bioelectronic sutures for the monitoring of deep surgical wounds," *Nat. Biomed. Eng.*, vol. 5, no. 10, pp. 1217–1227, 2021.

[24] S. S. Karipott, B. D. Nelson, R. E. Guldberg, and K. G. Ong, "A wireless, battery-free embedded sensor for monitoring tension on a suture anchor," *IEEE Sensors J.*, vol. 22, no. 2, pp. 1173–1179, 2021.

[25] K. M. Meyers, and K. G. Ong, "Pledget sensor to monitor loading in tendon and ligament sutures during postoperative physical therapy," *IEEE Sensors J.*, vol. 22, no. 19, pp. 18384–18390, 2022.

[26] J. Liang, L. Guo, C. C. Chiau, and X. Chen, "CPW-fed circular disc monopole antenna for UWB applications," in *Proc. IEEE Int. Workshop Antenna Technol. (iWAT),* Singapore, 2005, 505–508.

[27] S. Gabriel, R. W. Lau, and C. Gabriel, "The dielectric properties of biological tissues: II. Measurements in the frequency range 10 Hz to 20 GHz," *Phys. Med. Biol.,* vol. 41, no. 11, pp. 2251–2269, 1996.